Appl Phys A (2009) 96: 189–196
DOI 10.1007/s00339-008-4986-0

Applied Physics A
Materials Science & Processing

INVITED PAPER

Photographic diagnosis of crystalline silicon solar cells utilizing electroluminescence

Takashi Fuyuki · Athapol Kitiyanan

Received: 12 January 2008 / Accepted: 4 November 2008 / Published online: 11 December 2008

Abstract The photographic surveying of electroluminescence (EL) under forward bias was proved to be a powerful diagnostic tool for investigating not only the material properties but also process induced deficiencies visually in silicon (Si) solar cells. Under forward bias condition, solar cells emit infrared light (wavelength around 1000 to 1200 nm) whose intensity reflects the number of minority carriers in base layers. Thus, all the causes that affect the carrier density can be detected, i.e., the minority carrier diffusion length (or in other words, lifetime), recombination velocity at surfaces and interfaces, etc. (intrinsic material properties), and wafer breakage and electrode breakdown, etc. (extrinsic defects). The EL intensity distribution can be captured by Si CCD camera in less than 1 s, and the detection area simply depends upon the optical lens system suitable to the wide range of 1 cm–1.5 m. This fast and precise technique is superior to the conventional scanning method such as the laser beam induced current (LBIC) method.

The EL images are displayed as grayscale, which leads to the difficulty of distinguishing the sorts of those deficient areas. Since the intrinsic deficiency is more sensitive to temperature than the extrinsic deficiency, the change in solar cell temperature can offer the difference in EL intensity contrasts. These effects upon the measurement temperature can be applied to categorize the types of deficiency in the crystalline Si solar cell.

PACS 78.60.Fi · 73.40.Lq · 72.40.+w

T. Fuyuki (✉) · A. Kitiyanan
Graduate School of Materials Science, Nara Institute of Science and Technology, 8916-5 Takayama, Ikoma, Nara 630-0192, Japan
e-mail: fuyuki@ms.naist.jp
Fax: +81-743-726078

1 Introduction

According to a very large scale production of crystalline Si solar cells, serious problems, such as wafer cracking, breakage, or electrode breakdown, are of major concern. Thus, quick and precise evaluations of solar cell production are strongly required to obtain high efficiency and reliable performance of crystalline Si cells reproducibly under mass production process. For the detailed characterization and optimization of cell performance, the most important material parameter to be analyzed is the minority carrier diffusion length (or life time) which governs the short circuit current and open circuit voltage. Beside the conventional methods, such as the photoconductivity decay [1], the spectroscopic laser beam induced current (LBIC) [2], and the electron beam induced current (EBIC) methods [3], we have proposed an electroluminescence (EL) imaging technique [4] to analyze the minority carrier diffusion length distribution in as-fabricated cells or modules. The EL imaging technique has recently been demonstrated to be a powerful and fast characterization tool providing spatially resolved information about the electronic material properties of solar cells. This technique has been further developed for a more quantitative analyses of the effective diffusion length by the collection efficiency analysis in the absorption of near bandgap light [5, 6] and the local series resistance [7].

A cooled Si-CCD camera was used to capture the EL (infrared light, wavelength around 1000 to 1200 nm) which was emitted by a solar cell under forward bias condition. The EL intensity distribution clearly agreed with the mapping of minority carrier diffusion length in the samples [4], since the EL intensity was proportional to the total excess minority carrier density. Inhomogeneities caused by dislocations and/or grain boundaries could be visually shown.

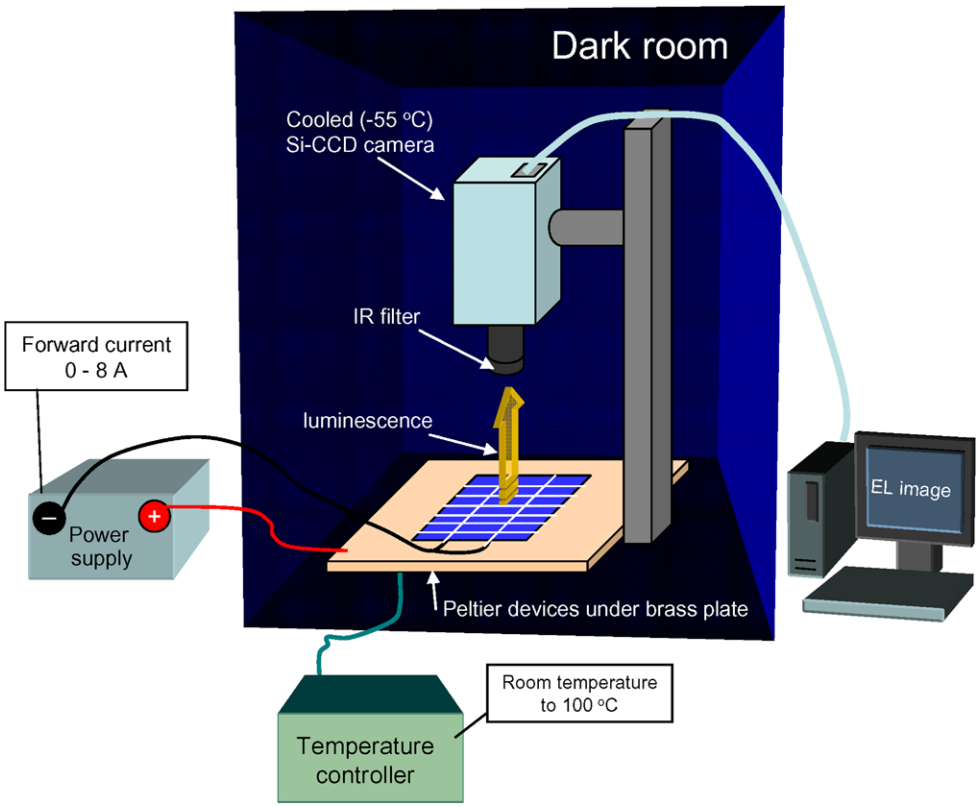

Fig. 1 A schematic viewgraph of experimental setup

Process induced deficiencies such as defects and cracks reduced the minority carrier density and could also be detected spatially as dark parts (spot, line, and area) on EL images [8–10].

The EL image was displayed in a grey scale which led to the difficulty of distinguishing the sorts of those deficient areas. Thus, other approaches had to be considered in order to identify the sorts of deficient parts effectively. Since dislocations, grain boundaries, etc. (intrinsic deficiency) are more sensitive to temperature than cracks, broken fingers or process-induced defects (extrinsic deficiency), the variation in measurement temperature of EL could offer the difference in EL intensity contrasts. In the case of multi-crystalline Si solar cell, the EL images at high temperature (100°C) displayed much lower contrasts at the intrinsic defects areas, while the contrasts around external faults areas seemed to be the same when compared to the EL image at room temperature [10]. Thus, these differences could be effective to distinguish the intrinsic and extrinsic deficiencies in solar cells.

2 Experimental

The solar cell under investigation was biased at an appropriate forward bias voltage. The emitted photons due to radiative band-to-band recombination have a peak luminescence at around 1150 nm corresponding to the silicon bandgap. The photons were collected by a Si CCD camera with 512 × 512 pixels cooled at −50°C. Forward bias voltage was applied to the sample to get the current of around 40 mA/cm^2, which corresponded to the typical short circuit current under 1 sun solar irradiation. The experiment was done in the dark room. The data acquisition time was chosen in the range of 0.1 and 2 seconds. Spatial resolution of analysis was limited by the optical system and varied based on the magnification scale of the frame.

In front of the camera lenses, an optical IR long pass filter with a cut-off wavelength of 850 nm was used to reduce the disturbance of surrounding light. For the temperature dependent analysis, the sample stage was equipped with four Peltier heaters allowing sample temperatures from room temperature to 100°C with lateral variations of 0.5°C (15 cm square area). The experimental apparatus setup is schematically shown in Fig. 1.

3 Electroluminescence images

The typical emission spectrum of a sample at room temperature, which was taken by an infrared sensitive Ge photodetector cooled at liquid nitrogen temperature, is shown as the dashed line in Fig. 2. The dominant peak was found at 1150 nm, which was the band-to-band radiative recombination assisted by phonons [8]. The sensitivity of the Si-CCD

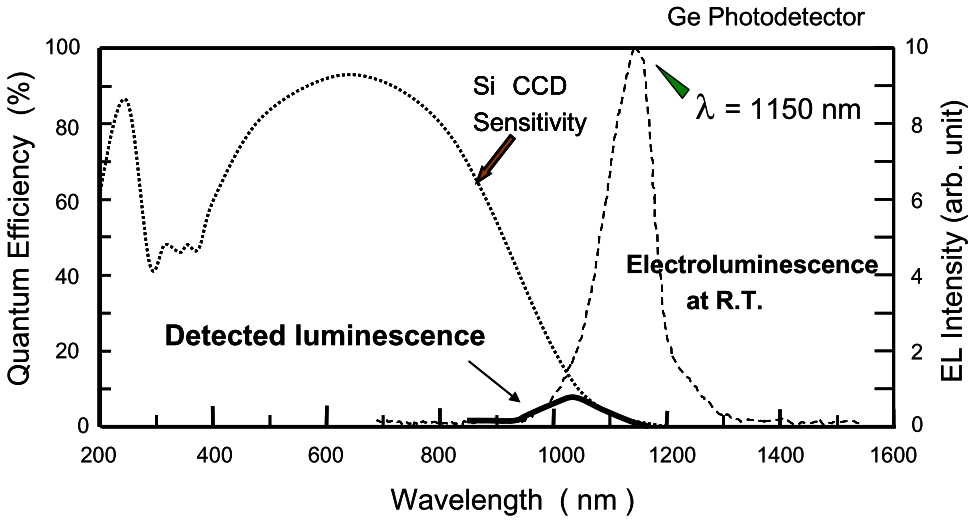

Fig. 2 A typical emission spectrum and the sensitivity of the Si-CCD camera

was up to 1200 nm as shown by the dotted line in Fig. 2. Thus, the limited portion of emission (schematically shown by the bold solid line with a peak at 1050 nm) could be detected by this system. In addition, the absorption coefficient of Si at 1050 nm is 16.3 cm^{-1} in Si, and so re-absorption of emission was negligible in the case of typical Si cells with a thickness of 200–300 μm.

The EL emission at room temperature from the forward biased mono-crystalline silicon solar cell is shown in Fig. 3. Homogeneous solar cell performance due to uniform diffusion length would result in an EL image without any spatial variations or inhomogeneities, see Fig. 3b. Figure 4 illustrates the optical and EL images of a commercially available multi-crystalline Si solar cell in Fig. 4a and b, respectively. Dislocation clusters and grain boundaries in multi-crystalline Si solar cell became visible clearly as shown in Fig. 4b.

4 Process-induced defect detection

4.1 Broken finger and crack detection

Figure 5 illustrates the optical and EL images of a mono-crystalline Si solar cell. In the bottom part of Fig. 5b, a long horizontal line (shown using the circular mark) could be observed in the EL image. This was caused by the wafer crack which could not be observed in the optical image of Fig. 5a.

The EL imaging technique could be used to detect broken fingers as shown by dashed squares in Fig. 5b. The magnified EL image of the area M1 in Fig. 5b is shown in Fig. 5c. The insert shows the magnified optical photography of the selected finger no. 51 and clearly exposes the broken part of finger no. 51. The EL method is an easy and quick way to detect the process failure simply by checking the reduction of EL intensity. Figure 5d shows the horizontal line scan as indicated by the arrow in Fig. 5c across the broken finger no. 51. From the line scan profile, this disconnection resulted in potential drops between fingers no. 50 and 52, and the broken finger did affect not only the area beneath finger but also the vicinity.

4.2 Quality of metal fingers contact

The low quality finger contact increases series resistance between finger and emitter layer of a finished cell, and the control of the so-called fire-through process and/or annealing process are of concern in mass-production. Figure 6 illustrates the zoomed EL images of some part of a mono-crystalline Si solar cell. Figure 6a was taken under low forward current (6.4 mA/cm^2) applied to the sample. The trace of miss-contacted finger is displayed on the left side of this figure as a shallow dark region, while other parts of the cell do not show inhomogeneities. At an increased forward current (51.2 mA/cm^2), inhomogeneity along the miss-contacted finger became clear as the dark shadow area in Fig. 6b. This indicates that high series resistance took place along the finger due to low quality metallic contact.

4.3 Solar cell module fabrication failure

The EL imaging technique could be applied not only to the cell but also to the fabricated modules and panels. The resolution and magnification of EL images depended on the focal length of optical lens and the distance between Si-CCD camera and solar cell sample. Figure 7 illustrates the EL images in the case of a large size (75 × 150 cm^2) commercial module. This image displays locations of low quality cells and/or process-induced defects which could occur in a module fabrication process. As shown in Fig. 7b, the point-pressure cracks due to the failure in the metal wire soldering could be observed in the EL image but we could not detect them in the usual optical image.

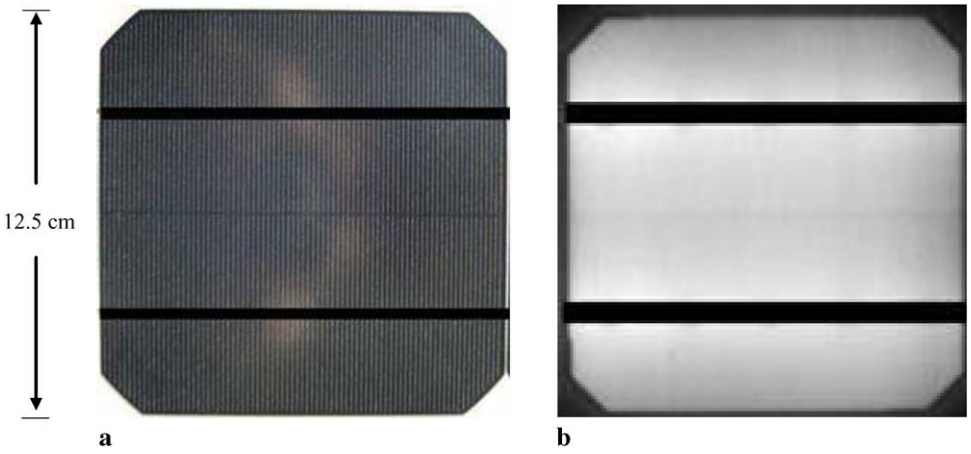

Fig. 3 Monocrystalline Si cell without any spatial variations as a reference: **a** optical image, **b** EL image under forward current density of 35 mA/cm^2

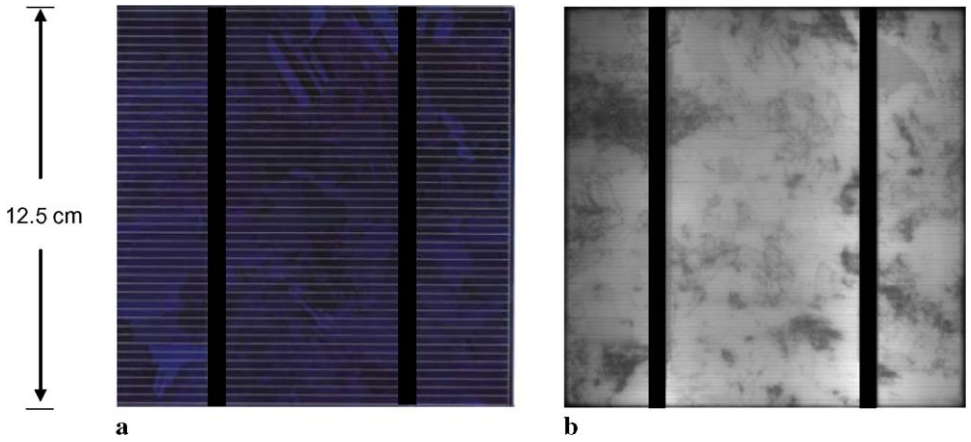

Fig. 4 Commercially available multicrystalline Si solar cell: **a** optical image, **b** EL image

5 EL dependence on forward voltage

The excess minority carrier distribution under forward bias is schematically shown in Fig. 8. The total excess minority carrier number N along the depth x in the bulk is expressed as

$$N = \int_0^w n_{p(o)} \exp(-x/L_e)\, dx = n_{p(o)} L_e, \tag{1}$$

where $n_{p(o)}$ is the excess minority carrier number at the p–n junction edge, L_e is the effective diffusion length, and w is the width of p base layer.

The electroluminescence intensity, I_L, was considered to be proportional to N integrated along the depth, and then to L_e at the fixed injection condition $n_{p(o)}$. The EL intensity was also proportional to $n_{p(o)}$, which was governed by the applied forward voltage V_f (equal to the quasi-Fermi level difference of the minority carrier) by the following equation:

$$n_{p(o)} = n_p \exp(eV_f/kT), \tag{2}$$

where n_p, e, k, and T are the equilibrium minority carrier density in the p layer, electron charge, Boltzmann constant, and measurement temperature, respectively. Thus, when the forward current was varied, I_L could be expressed as a function of V_f as follows:

$$I_L = A \exp(eV_f/kT), \tag{3}$$

or

$$\ln I_L = A' + (e/kT)V_f, \tag{4}$$

when A, A': constant.

In Fig. 9, the dark current (I)–forward voltage (V_f) curve from the experimental (square marks) was fitted with the 2-diode-model calculated by the PC1D simulator (bold line). The calculated dark I–V_f by neglecting the effects of diode saturation current densities of $n = 2(J_{02})$ and shunt resistance (R_{sh}), which is shown as a dashed straight line, was in good agreement with the experimental semi-log plot of I_L and V_f (shown by circle marks). This result suggests that $\ln I_L$ increased linearly with V_f in the whole range, and the slope was e/kT as expected from (4). The relationship between the electroluminescence intensity and the forward voltage yielded the convenient technical method that the open circuit voltage of solar cell could be derived easily by comparing the EL intensities of different solar cells at the constant injection current level [9].

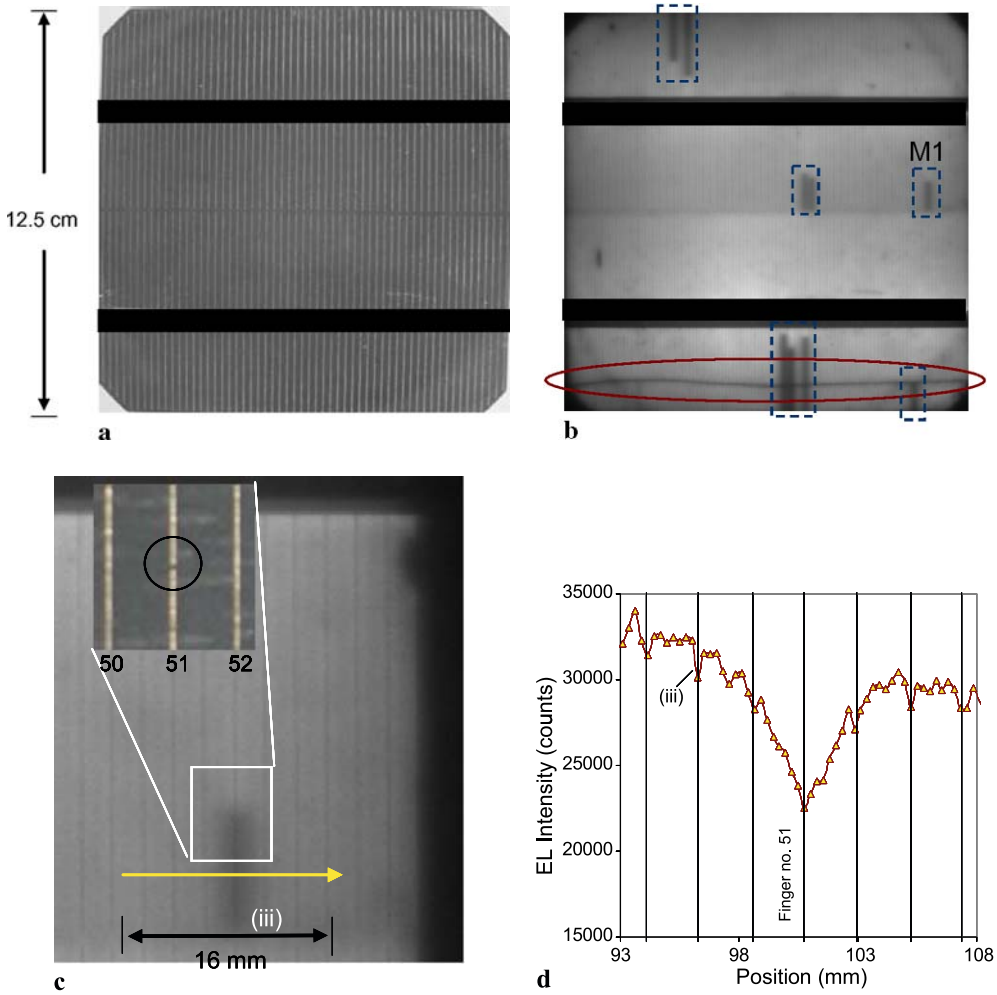

Fig. 5 Images in the case of a defected monocrystalline Si cell: **a** optical image, **b** EL image of the sample under forward current density of 35 mA/cm^2, **c** magnified EL image of the *middle right part* (area M1 of **b**), **d** EL intensity profile of a line scan which is indicated by an *arrow (iii)* in **c**

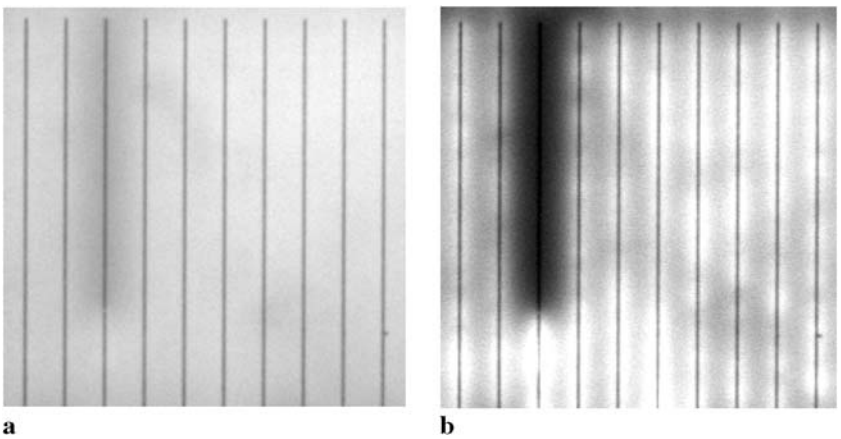

Fig. 6 EL images of broken metal finger contacts: **a** under forward current of 6.4 mA/cm^2, **b** under forward current of 51.2 mA/cm^2

6 EL measured at elevated temperatures

As mentioned above, the EL imaging technique could be a powerful tool for solar cell characterization. However, the quality of the specific areas in EL images was poor since those areas were displayed in a grayscale which led to the difficulty of distinguishing the sorts of those deficient areas. Thus, other approaches had to be considered in order to identify the sorts of deficient parts effectively.

The temperature has a larger effect on the intrinsic deficiency (crystallographic defects and grain boundaries, etc.) than the extrinsic deficiency (wafer breakage, etc.) since the minority carrier diffusion length and lifetime depend upon the electronic levels of traps. Very deep traps at extrinsic de-

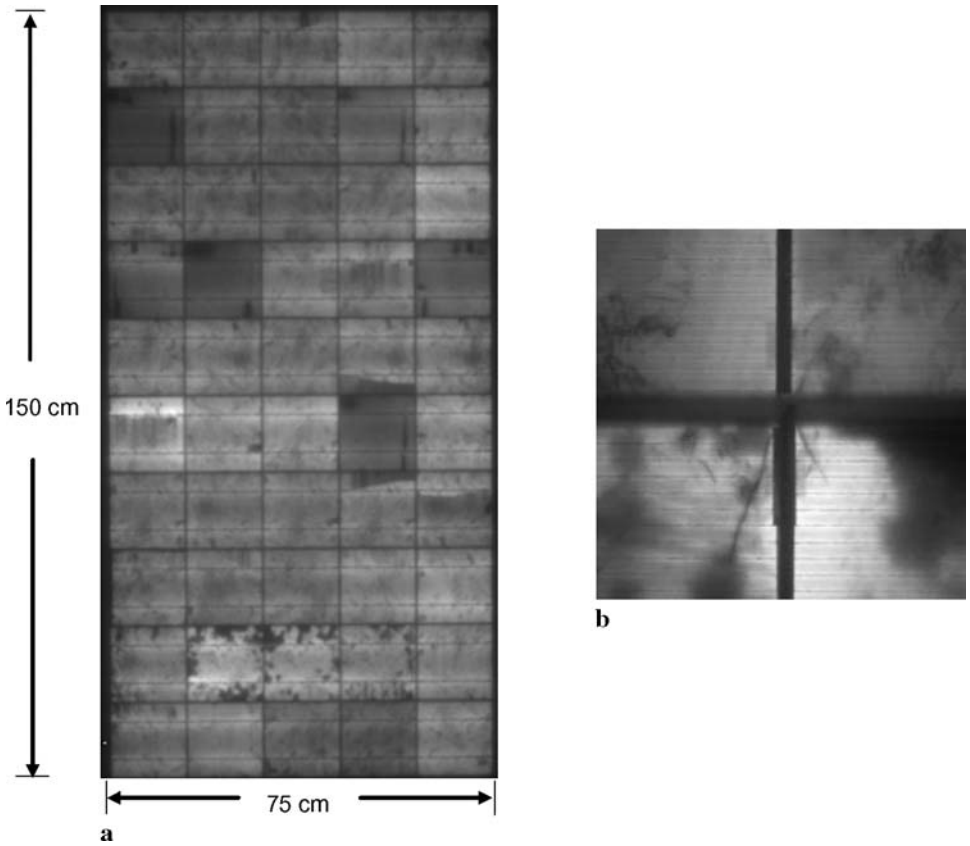

Fig. 7 EL images of solar cell module **a** and "point-pressure crack" failure due to metal wire soldering **b**

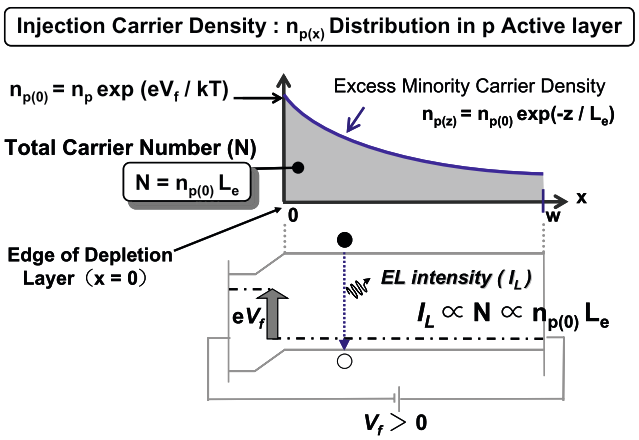

Fig. 8 A schematic viewgraph of excess minority carrier density distribution in the typical n^+p Si solar cell

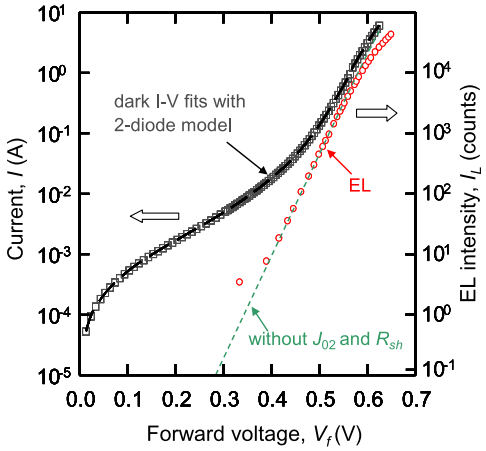

Fig. 9 Simulated dark current (I)–voltage (V_f) curve fitted to the experimental data, and semilogarithmic plot of EL intensity (I_L) as a function of forward voltage V_f

fects have less sensitivity in the temperature variation in this range (25–100°C). The change in measurement temperature could offer the difference in EL intensity patterns [11]. Figure 10 illustrates the EL images of a multi-crystalline Si solar cell at different temperatures. At higher temperatures, the lower contrast could be observed in many deficient locations (dark parts). For the solar cell investigated in this study we did not expect lateral variations in the rear surface recombination velocity or the emitter sheet resistance at the front. All the lateral variations in the temperature dependence of the EL were expected to arise from local variations in the temperature dependence of the bulk recombination properties [12].

To clarify the temperature affected locations, the image processing technique was applied by subtracting two EL images at different temperatures. The subtracted image was produced from the intensity at high temperature (100°C)

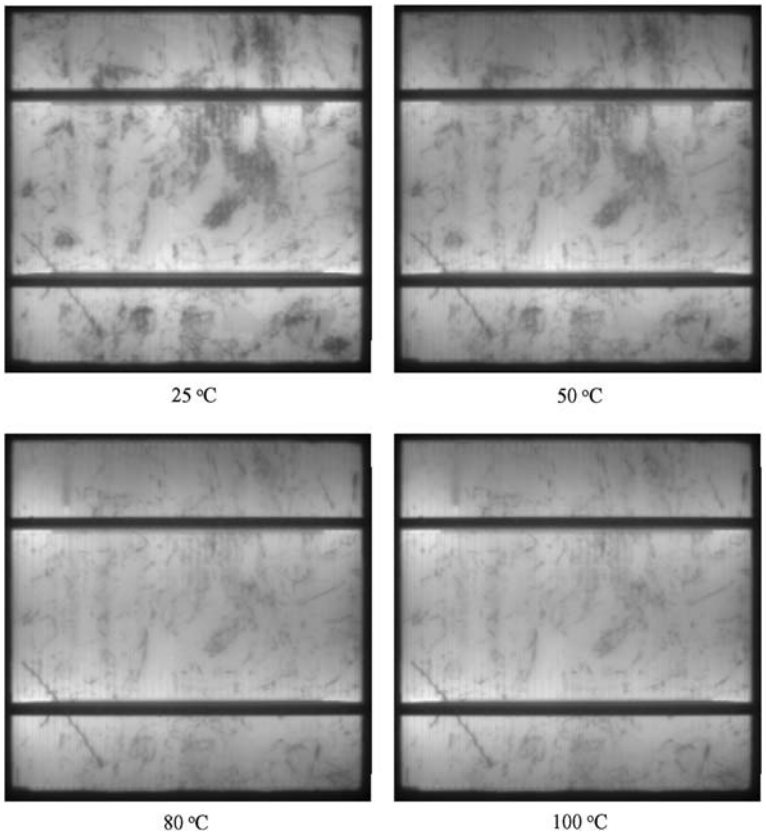

Fig. 10 EL images of a multi-crystalline Si solar cell at different temperatures

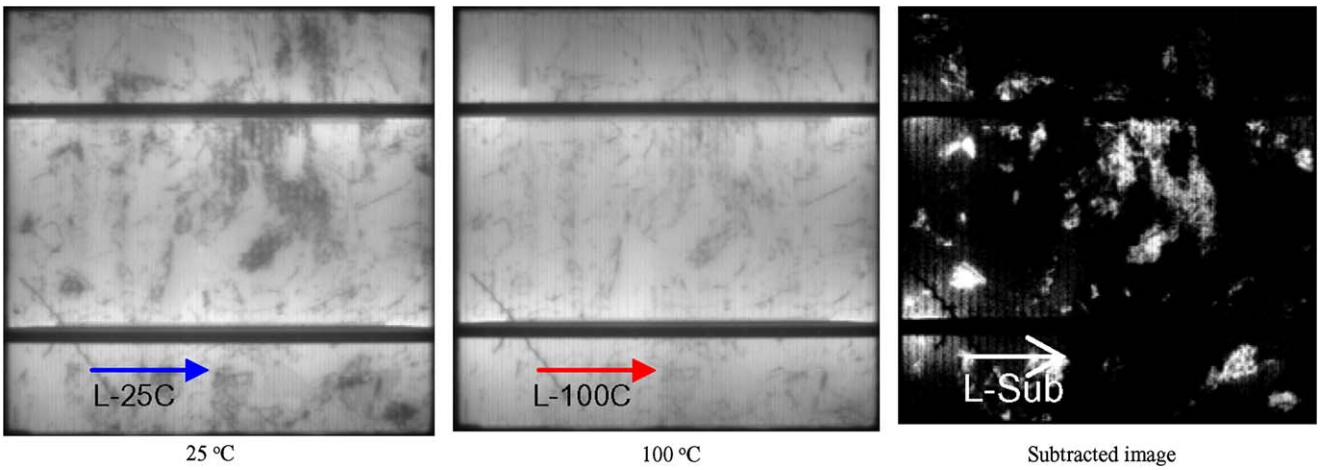

Fig. 11 Processing by subtraction of temperature different EL images between 100°C and 25°C

minus the intensity at lower temperature (25°C) performed pixel by pixel.

Figure 11 presents the EL images of the sample at 25°C, 100°C, and the subtracted images. The subtracted image illustrates that the brighter areas correspond to the areas which were strongly affected by the change of temperature. For the block-cast multi-crystalline silicon, the EL signal near and in regions of high dislocations was strongly affected by the temperature variation. The brighter areas were considered to indicate the intrinsic defects locations in the subtracted image.

The three scanned lines, L-25C, L-100C and L-Sub, at the same track and scanned from left to right through the cracked position (around pixel no. 20) and defect parts (at almost the end of the scanned line) in Fig. 11 are shown in Fig. 12 in the plots of position (in pixel) versus EL intensities. From the plots in Fig. 12, at 25°C (L-25C), the EL intensity at both the cracked position and defected areas was

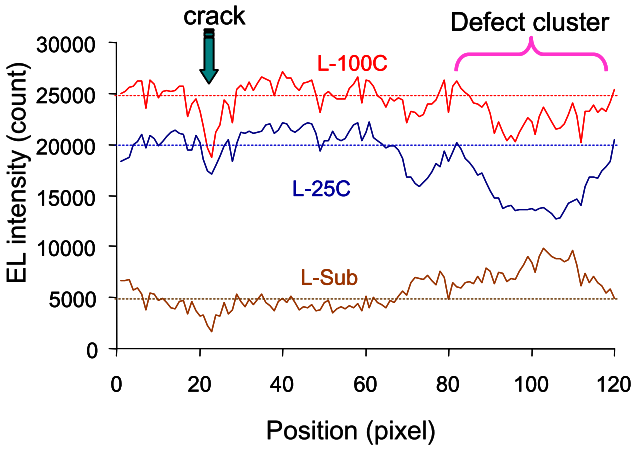

Fig. 12 Line scan profiles of EL intensity. The lines of L-25C, L-100C and L-sub correspond to the arrows shown in Fig. 11

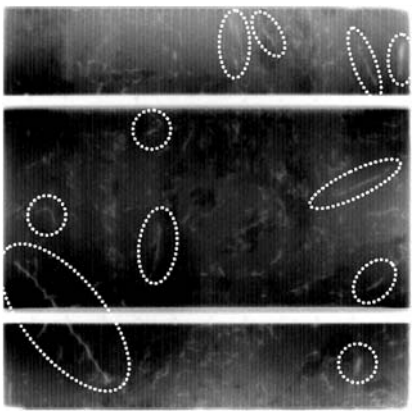

Fig. 13 An EL image of extrinsic deficiencies indicated by *dashed circular marks*

much lower than the average value (avg. ∼20 000 counts). In contrast to the room temperature (25°C), the EL intensity around defect area in the line scan L-100C was approximately the same as the average value (avg. ∼24 500 counts), while that of the cracked position still showed a very low intensity. The L-Sub line is the plot of the EL intensity which was obtained from L-100C by subtracting L-25C point by point. The obtained difference showed that the defect area gave the higher intensity than that at the cracked position. This led to the difference in contrast between defect areas and cracked position in the subtracted image.

After performing an appropriate image processing technique, the extrinsic deficiency image could be obtained as shown in Fig. 13. This image emphasized the locations of the process induced defects in multi-crystalline solar cell sample.

7 Conclusions

The electroluminescence imaging technique provided the information about the electrical and material properties of solar cells. The cracks or defect clusters and also the positions of broken fingers in solar cells could be detected very fast and clearly as dark parts or inhomogeneities in the EL images. In addition, the EL imaging technique could be used to evaluate the large size solar cell modules within one second of exposure time which makes this technique an ideal in-line diagnostic tool for crystalline silicon solar cells and modules production. The image subtraction of two different temperature EL images was performed in order to distinguish the intrinsic and extrinsic deficiencies in multi-crystalline Si solar cells. This electroluminescence imaging combined with the temperature difference subtraction technique should be a versatile tool to categorize deficient areas in crystalline Si solar cell and be suitable for the quality control for the solar cell production.

Acknowledgements Funding for this work is partially supported by NEDO. Fruitful discussions and valuable data from Dr. Karsten Bothe are gratefully acknowledged.

References

1. J.A. Eikelboom, C. Leguijt, C.F.A. Frumau, A.R. Burgers, Sol. Energy Mater. Sol. Cells **36**, 169 (1995)
2. O. Porre, M. Stemmer, M. Pasquinelli, Mater. Sci. Eng. B **24**, 188 (1994)
3. W. Seifert, M. Kittler, J. Vanhellemont, Mater. Sci. Eng. B **42**, 260 (1996)
4. T. Fuyuki, H. Kondo, T. Yamazaki, Y. Takahashi, Y. Uraoka, Appl. Phys. Lett. **86**, 262108 (2005)
5. P. Wurfel, T. Trupke, J. Appl. Phys. **101**, 123110 (2007)
6. K. Bothe, D. Hinken, K. Ramspeck, B. Fischer, R. Brendel, in *Proceedings of the 22nd European Photovoltaic Solar Energy Conference 2007*, Milan (2007), pp. 1673
7. D. Hinken, K. Bothe, K. Ramspeck, B. Fischer, R. Brendel, Appl. Phys. Lett. **91**, 182104 (2007)
8. Y. Takahashi, Y. Kaji, A. Ogane, Y. Uraoka, T. Fuyuki, in *Proceedings of the 4th World Conference on Photovoltaic Energy Conversion 2006*, Hawaii, 2006
9. T. Fuyuki, H. Kondo, Y. Kaji, A. Ogane, Y. Takahashi, J. Appl. Phys. **101**, 023711 (2007)
10. A. Kitiyanan, K. Bothe, Y. Takahashi, A. Ogane, T. Fuyuki, in *Proceedings of the 22nd European Photovoltaic Solar Energy Conference 2007*, Milan (2007), pp. 1387
11. A. Kitiyanan, K. Bothe, Y. Takahashi, A. Ogane, T. Fuyuki, in *Technical digest of the 17th International Photovoltaic Science and Engineering Conference 2007*, Fukuoka (2007), pp. 706
12. K. Bothe, D. Hinken, K. Ramspeck, A. Kitiyanan, T. Fuyuki, in *Technical digest of the 17th International Photovoltaic Science and Engineering Conference 2007*, Fukuoka (2007), pp. 261